Polymer Chemistry

RSC Publishing

PAPER

View Article Online
View Journal | View Issue

Cite this: *Polym. Chem.*, 2013, **4**, 4162

Linkage and acceptor effects on diverse memory behavior of triphenylamine-based aromatic polymers†

Chih-Jung Chen, Yi-Cheng Hu and Guey-Sheng Liou*

Received 18th April 2013
Accepted 10th May 2013

DOI: 10.1039/c3py00500c

www.rsc.org/polymers

A new functional triphenylamine-based (TPA-based) aromatic polyether (**OXPE**) derived from 2,5-bis(4-fluorophenyl)-1,3,4-oxadiazole and 4,4′-dihydroxytriphenylamine and polyester (**6FPET**) derived from 4,4′-(hexafluoroisopropylidene)bis(benzoyl chloride) and 4,4′-dihydroxytriphenylamine were synthesized and used for memory device applications. To get more insight into the relationship between the linkage group and memory behavior, polyamide **6FPA**, polyimide **6FPI**, and the corresponding isomer **6FPI′** were also synthesized and their memory properties were investigated. The linkage effects of polyether, polyester, polyamide, and polyimide are expected to reveal different retention times of the synthesized polymer memory devices due to their different structural conformations, dipole moments, HOMO, and LUMO energy levels. **OXPE**, **6FPA**, and **6FPET** with a non-planar linkage structure but different LUMO energy levels possess SRAM behavior with different retention times, 2 min, 5 min, and 6 min, respectively. **6FPI** with a planar linkage group exhibits DRAM property while the corresponding isomer **6FPI′** reveals insulator behavior due to the difficulty in sustaining the charge transfer complex. Furthermore, to illustrate the linkage and acceptor effect systematically, TPA-based sulfonyl-containing polymers with the same linkages were also added into the discussion.

Introduction

Due to the exponential growth of information and communication and the miniaturization of electronic devices, polymeric memory materials have attracted increasing attention over the years since the first one published by Sliva *et al.* in 1970.[1] Comparing with conventional inorganic memory materials, polymeric materials have numerous advantages such as ease of miniaturization, tailored properties through molecular design, low-cost, solution processability, flexibility, and three-dimensional stacking capability for practical use.[2] As a promising alternative to inorganic semiconductor-based memory, polymeric memory materials store information in the form of high (ON) and low (OFF) current states in place of the amount of charges stored in a cell of silicon devices. In the starting stage of polymer memory applications, polymers were used as polyelectrolytes or matrices in a doped system.[3] To advance the function of polymers for memory devices further, the design and synthesis of the polymers with specific structures that can provide expected memory properties within a single polymer chain is an important and crucial issue.

For resistive type memory materials, electron donor–acceptor polymers are considered as suitable materials because charge transfer (CT) between the donor and acceptor moieties can give rise to a highly conductive state.[4] Donor–acceptor type polymers including conjugated polymers,[5] non-conjugated pendent polymers,[6] polymer composites,[7] and functional polyimides[8] have been reported widely with all kinds of chemical structures. Among all the studied donor–acceptor systems, aromatic polyimides are promising candidates for memory device applications due to the excellent thermal dimensional stability, chemical resistance, mechanical strength, and high ON/OFF current ratio resulting from the low conductivity in the OFF state. Although aromatic polyimides have superior properties, they are generally restricted by limited solubility in most organic solvents and their high glass transition (T_g) or melting temperatures caused by the high crystallinity and high stiffness of the polymer backbones, and charge transfer complex formation. To overcome the solubility problem of polyimides, the non-coplanar triphenylamine (TPA) group was introduced into polyimides and enhanced the solution processability. Furthermore, TPA could act as a donor and facilitate the CT behavior of polyimide, therefore, a series of TPA-based polyimides with different substituted groups and dianhydrides were prepared for memory devices.[4a,9]

In addition to polyimides, TPA-based aromatic polyamides and polyesters were also characterized as highly thermally

Functional Polymeric Materials Laboratory, Institute of Polymer Science and Engineering, National Taiwan University, 1 Roosevelt Road, 4th Sec., Taipei 10617, Taiwan. E-mail: gsliou@ntu.edu.tw

† Electronic supplementary information (ESI) available: Figure: IR spectra, TGA thermograms, and DSC traces of polyether OXPE and polyester 6FPET. Reduction cyclic voltammetric diagrams of **6FPI** and **6FPI′**, and simulation results of TPA-based sulfonyl-containing polymers. Table: molecular weights and solubility behavior. See DOI: 10.1039/c3py00500c

stable polymers with a favorable balance of physical and chemical properties.[10] In our previous study, TPA-based polyamide and polyester revealed different volatile memory characteristics from polyimide due to the difference of linkage, dipole moment, HOMO, and LUMO energy levels among these polymers.[11] In addition to the conformational changes of the flexible linkage between the donor and acceptor moieties of the aromatic polyamide and polyester, the increment of torsional displacement induced by charge transfer would produce a potential energy barrier for the back charge transfer that resulted in the longer retention time.[12] It is interesting to get more insight into the relationship between memory behaviors and linkage groups of these functional polymers.

Furthermore, TPA-containing aromatic polyethers could also be obtained as high performance polymers with excellent processability, electroactive and electrochromic properties.[13] However, in our previous study, TPA-based sulfonyl-containing polyether **DSPE** exhibited only insulator behavior due to the large band gap and weak CT capability.[11b] According to previous literature, memory devices with thinner thickness are advantageous to reduce switch-on voltage and reveal memory behavior.[9b,9c,11a] In this study, we therefore synthesized oxadiazole-containing polyether **OXPE** derived from 2,5-bis(4-fluorophenyl)-1,3,4-oxadiazole and 4,4′-dihydroxytriphenylamine with a stronger acceptor moiety than **DSPE**, and also reduced film thickness of the resulting polyethers to achieve the memory characteristics for the first time. TPA-containing polyimides could be synthesized either from TPA-based diamine or TPA-based dianhydride to have different directions of polyimide linkages. We also predicted that the direction of polyimide linkages could affect the CT behavior and the resulting memory property. Therefore, the corresponding isomer **6FPI′** of **6FPI** was synthesized in this present work to demonstrate the isomeric effect on the memory property. In order to illustrate the linkage and acceptor effect systematically, polyamide **6FPA** and the new functional polyester **6FPET** derived from 4,4′-(hexafluoroisopropylidene)bis(benzoyl chloride) and 4,4′-dihydroxytriphenylamine were prepared for detailed discussion and compared with the corresponding sulfonyl-containing polymers.

Results and discussion

Polymer synthesis and characterization

The TPA-based new polyether **OXPE** was prepared by the reaction of diol monomer **1** with **OXDF** in NMP at 150 °C with toluene to remove water during the formation of phenoxide anions, followed by 170 °C, 180 °C, and 190 °C reaction temperature segments as shown in Fig. 1. The formation of polyether **OXPE** was confirmed by IR spectroscopy showing characteristic absorption bands at around 1500–1600 (C=N), and 1232 cm^{-1} (C–O–C) (Fig. S1a†). Anal. calcd (%) for **OXPE** C, 77.56; H, 4.27; N, 8.48 and found C, 75.11; H, 3.82; N, 8.27. The TPA-based new polyester **6FPET** was synthesized by the reaction of diol monomer **1** (ref. 14*a*) with **6FAC** in *o*-dichlorobenzene at 180 °C as shown in Fig. 1. The formation of polyester **6FPET** was also confirmed by IR spectroscopy showing a characteristic ester carbonyl absorption band at around 1737 cm^{-1} (C=O) (Fig. S1b†). Anal. calcd (%) for **6FPET** C, 66.35; H, 3.34; N, 2.21 and found C, 64.56; H, 2.93; N, 2.15. Synthesis and

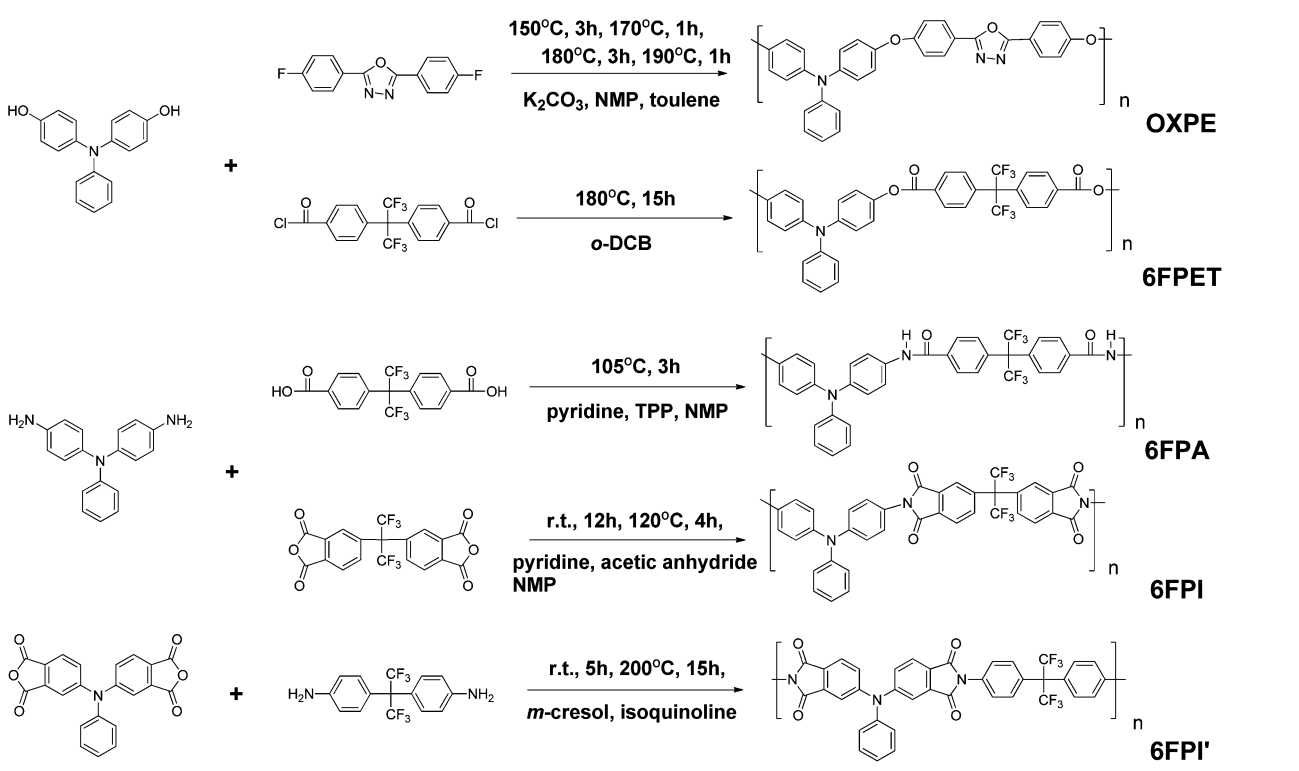

Fig. 1 Synthesis methods of **OXPE**, **6FPET**, **6FPA**, **6FPI**, and **6FPI′**.

characterization of **6FPA**, **6FPI**, and **6FPI′** have been described previously.[14c,15] The inherent viscosity and GPC analysis data of the TPA-based aromatic polymers are summarized in Table S1.† The obtained polymers have inherent viscosities in the range of 0.27–0.75 dL g^{-1} with weight-average molecular weights (M_w) and polydispersity (PDI) of 62 000–166 000 Da and 1.78–2.58, respectively, relative to polystyrene standard. The solubility behavior of **OXPE** and **6FPET** was investigated qualitatively and the results are listed in Table S2.† **OXPE** and **6FPET** exhibited excellent solubility not only in polar aprotic organic solvents such as NMP and DMAc, but also in less polar solvents such as $CHCl_3$ and THF. The excellent solubility can be attributed to the existence of the bulky TPA unit which limits the intermolecular interactions. The excellent solubility is conducive to fabricate the memory device by a solution process.

Thermal properties

The thermal properties of new functional polymers **OXPE** and **6FPET** were investigated by TGA and DSC, and the results are summarized in Table 1. Typical TGA and DSC curves of **OXPE** and **6FPET** are depicted in Fig. S2.† Both **OXPE** and **6FPET** exhibited good thermal stability with insignificant weight loss up to 350 °C under a nitrogen or air atmosphere. The 10% weight-loss temperatures of **OXPE** and **6FPET** were recorded to be 500 °C, 480 °C in nitrogen, and 500 °C, 465 °C in air, respectively. The amount of carbonized residue (char yield) of **OXPE** and **6FPET** in the nitrogen atmosphere was 49% and 50% at 800 °C, which could be ascribed to their high aromatic content. The Limiting Oxygen Index (LOI) of **OXPE** and **6FPET** calculated by the char yield was 37 and 38, respectively. The glass transition temperatures (T_g) of **OXPE** and **6FPET** were 206 °C and 193 °C, respectively. The excellent thermal properties were advantageous to the memory device which may release heat during operation.

Optical and electrochemical properties

UV-vis absorption spectra of **OXPE**, **6FPET**, **6FPA**, **6FPI**, and **6FPI′** are shown in Fig. 2 and the onset wavelengths of optical absorption were utilized to obtain the optical energy band gap (E_g) of these polymers. The electrochemical behavior of these

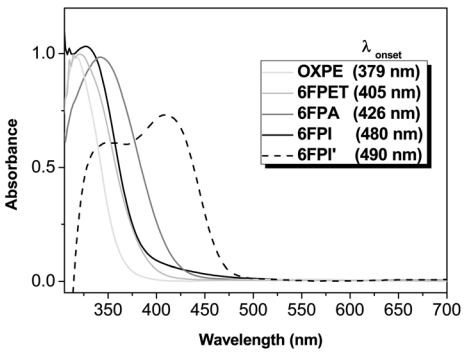

Fig. 2 UV-visible absorption spectra of **OXPE**, **6FPET**, **6FPA**, **6FPI**, and **6FPI′**.

polymers was investigated by cyclic voltammetry conducted by film cast on an ITO-coated glass substrate as the working electrode in dry acetonitrile (CH_3CN) containing 0.1 M of TBAP as an electrolyte under nitrogen atmosphere. The typical cyclic voltammograms for these polymers are depicted in Fig. 3. There is one oxidation redox couple for all polymers, and the onset oxidation of these five polymers exhibited at 0.69, 1.00, 0.71, 1.01, and 1.27 V, respectively. The optical and electrochemical properties of these five polymers are summarized in Table 2 along with TPA-based sulfonyl-containing polymers, and the optical energy band gaps (E_g) estimated from the onset optical absorption are 3.27, 3.06, 2.91, 2.58, and 2.53 eV, respectively. **6FPI** and **6FPI′** have similar low energy gaps due to the strong charge-transfer effect between the TPA moiety and the phthalic imide ring. The LUMO energy levels of these five polymers decrease in the order of **OXPE**, **6FPA**, **6FPET**, **6FPI**, and **6FPI′**. Reduction cyclic voltammograms were utilized to calculate the electrochemical LUMO energy levels of **6FPI** and **6FPI′** as shown in Fig. S3,† and the results are also summarized in Table 2. The HOMO energy levels of **OXPE**, **6FPET**, **6FPA**, **6FPI**, and **6FPI′** estimated from the onset of their oxidation in CV experiments were 5.13, 5.44, 5.15, 5.45, and 5.63 eV, respectively (on the basis of ferrocene/ferrocenium 4.8 eV below the vacuum level with E_{onset} = 0.36 V). Comparing the acceptor effect systematically, the corresponding sulfonyl-containing polymers generally have lower LUMO energy levels than hexafluoroisopropylidene-containing (6F) series polymers with the same linkage. Besides,

Table 1 Thermal properties

		T_d^{5c} (°C)		T_d^{10c} (°C)			
Polymer[a]	T_g[b] (°C)	N_2	Air	N_2	Air	R_{w800}[d] (%)	LOI[e]
OXPE	206	460	460	500	500	49	37
6FPET	193	450	420	480	465	50	38

[a] The polymer film samples were heated at 300 °C for 1 h prior to all the thermal analyses. [b] Midpoint temperature of baseline shift on the second DSC heating trace (rate: 20 °C min^{-1}) of the sample after quenching from 400 °C to 50 °C (rate: 200 °C min^{-1}) in nitrogen. [c] Temperature at which 5% and 10% weight loss occurred, respectively, recorded by TGA at a heating rate of 20 °C min^{-1} and a gas flow rate of 20 cm^3 min^{-1}. [d] Residual weight percentages at 800 °C under nitrogen flow. [e] LOI: limiting oxygen index = (17.5 + 0.4 × char yield).

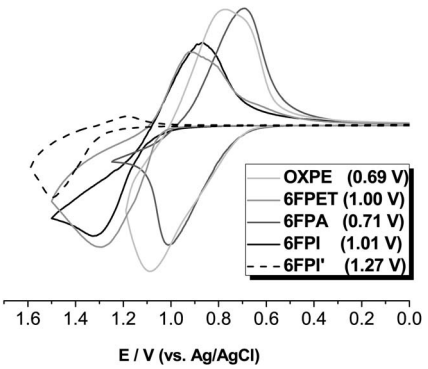

Fig. 3 Cyclic voltammetric diagrams of **OXPE**, **6FPET**, **6FPA**, **6FPI**, and **6FPI′** films on an ITO-coated glass substrate over cyclic scans.

Table 2 Redox potentials and energy levels of polymers

Polymer	Thin film (nm) λ_{onset}	Oxidation potential[a] (V) E_{onset}	E_g[b] (eV)	HOMO[c] (eV)	LUMO^{opt}[d] (eV)
OXPE	379	0.69	3.27	5.13	1.86
6FPET	405	1.00	3.06	5.44	2.38
6FPA	426	0.71	2.91	5.15	2.24
6FPI	480	1.01	2.58	5.45	2.87 (3.50)[e]
6FPI′	490	1.27	2.53	5.71	3.18 (3.46)[e]
DSPE	361	0.68	3.43	5.12	1.69
DSPET	458	1.01	2.71	5.45	2.74
DSPA	496	0.74	2.50	5.18	2.68
DSPI	567	1.02	2.19	5.46	3.27

[a] From cyclic votammograms *versus* Ag/AgCl in CH_3CN. [b] The data were calculated from polymer films by the equation: $E_g = 1240/\lambda_{onset}$ (energy gap between HOMO and LUMO). [c] The HOMO energy levels were calculated from cyclic voltammetry and were referenced to ferrocene (4.8 eV; $E_{onset} = 0.36$ V). [d] LUMO^{opt} (LUMO energy levels calculated from the optical method): difference between HOMO^{EC} and E_g^{opt}. [e] The LUMO energy levels were calculated from cyclic voltammetry and were referenced to ferrocene (4.8 eV; $E_{1/2} = 0.52$ V in DMF).

OXPE has lower LUMO energy levels than **DSPE** due to the stronger acceptor oxadiazole moiety.

Memory device characteristics

The memory behaviors of these TPA-based aromatic polymers were depicted by the current–voltage (*I–V*) characteristics of an ITO/polymer/Al sandwich device as shown in Fig. 4. Within the sandwich device, the polymer film was used as an active layer between Al and ITO as the top and bottom electrodes. To exclude the effect of the polymer film thickness on memory properties, a standard thickness (50 nm) was used without specific mention. Fig. 4a reveals *I–V* characteristics of **6FPET**. The device based on **6FPET** could not be switched to the ON state and stayed in the OFF state with a current range 10^{-13} to 10^{-14} A in the positive sweep up to 6 V (not shown). However, a sharp increase in the current could be observed at −3.6 V during the negative sweep, indicating that the device undergoes an electrical transition from the OFF state to the ON state (writing process). The device also remained in the ON state during the subsequent negative (the second sweep) and positive scans (the third sweep). Thus, this **6FPET** memory device could not be reset to the initial OFF state by the introduction of a reverse scan and is thus non-erasable. The fourth sweep was conducted after turning off the power for about 6 minutes and it was found that the ON state had relaxed to the steady OFF state without an erasing process. During the fourth sweep, the device could be switched to the ON state again at the threshold voltage of −3.3 V. Thus, the device could open to the ON state again and was rewritable. The 6 minutes retention time of **6FPET** memory device is indicative of volatile SRAM behavior.[12a] Fig. 4b reveals *I–V* characteristics of **6FPA** which have similar SRAM memory properties with different retention times of 5 minutes.

The memory device of **6FPI** switched from 10^{-13} to 10^{-14} to 10^{-5} A at the threshold voltage of −3.5 V in the negative sweep and the ON state could be read by the subsequent negative (the second sweep) and positive scans (the third sweep) as shown in

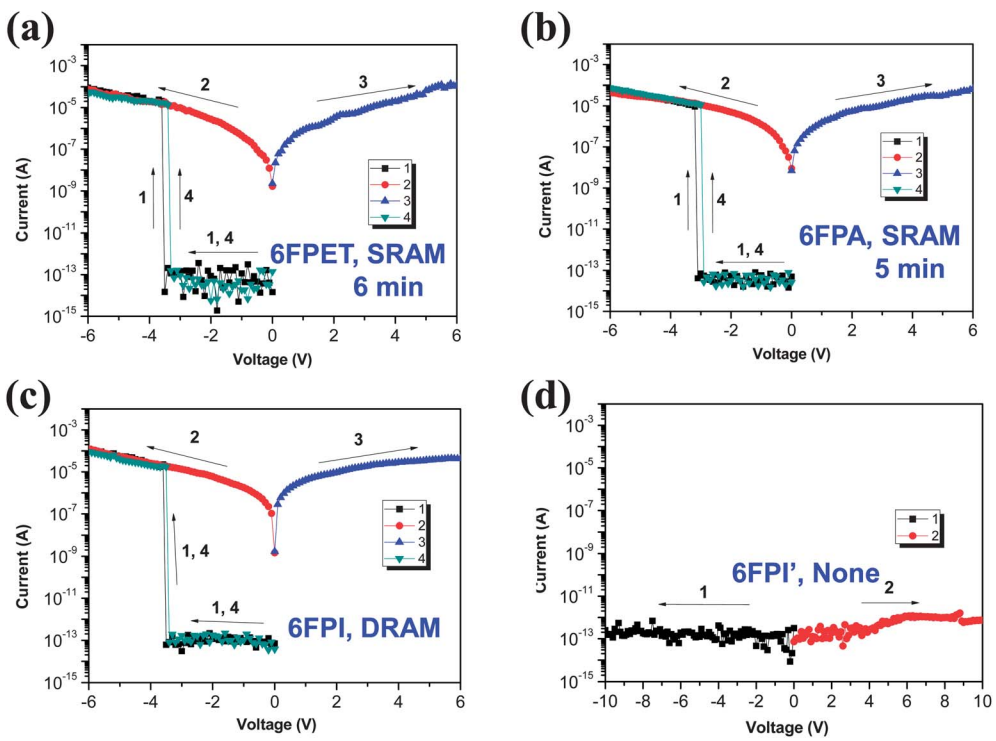

Fig. 4 Current–voltage (*I–V*) characteristics of the ITO/polymer (50 ± 3 nm)/Al memory device. (a) **6FPET**, (b) **6FPA**, (c) **6FPI** and (d) **6FPI′**.

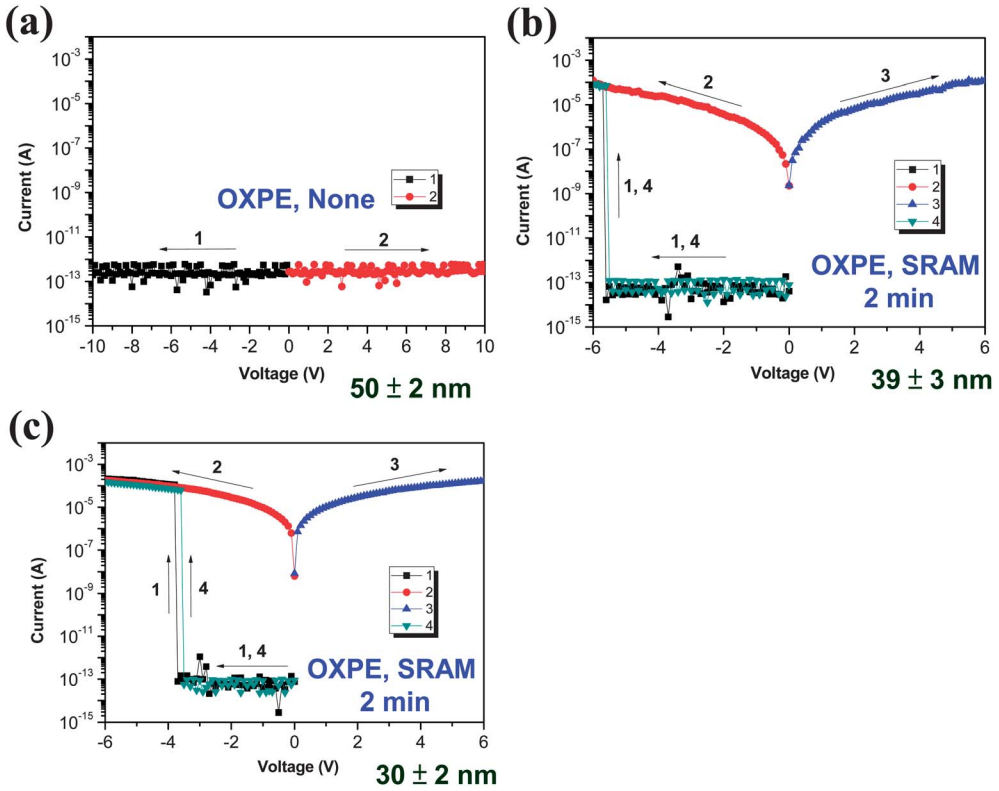

Fig. 5 Current–voltage (*I–V*) characteristics of the ITO/**OXPE**/Al memory device with different **OXPE** film thickness around (a) 50 nm, (b) 40 nm and (c) 30 nm.

Fig. 4c. The ON state would return to the OFF state in 1 min after removing the applied voltage and then subsequently switch to the ON state again at the threshold voltage of −3.4 V, implying similar volatile **DRAM** behavior to that published before.[4a] However, the corresponding **6FPI′** is maintained at the low-conductivity (OFF) state during the positive and negative scan as shown in Fig. 4d. Thus, **6FPI′** showed no memory but insulator behavior. Fig. 5 and 6 depict the *I–V* results of **OXPE** and **DSPE** with different thickness, respectively. **OXPE** exhibited insulator, SRAM, and SRAM properties with the corresponding thickness around 50, 40, and 30 nm, respectively. Meanwhile, **DSPE** only exhibited DRAM behavior with film thickness around 30 nm. Thus, these TPA-based aromatic polymers exhibited not only diverse memory properties but also high ON/OFF current ratios of 10^8 to 10^9. The high ON/OFF current ratio is advantageous to reduce misreading probability between the ON state and the OFF state.

Theoretical analysis and switching mechanism

In order to get more insight into the different memory behavior of the present TPA-based aromatic polymer devices, molecular simulation on the basic unit was carried out by DFT/B3LYP/6-31G(d) with the Gaussian 09 program. The charge density isosurfaces of the basic unit and the most energetically favorable geometry of **OXPE**, **6FPET**, **6FPA**, **6FPI**, and **6FPI′** are summarized in Fig. 7, and the simulation results of TPA-based sulfonyl-containing polymers are listed in Fig. S4.† The LUMO energy levels calculated by molecular simulation were in agreement with the experimental value tendency and could be utilized as evidence to indicate the electron-withdrawing intensity of various acceptors and donor–acceptor interaction capability *via* different linkage groups. For these TPA-based polymer systems, the HOMO energy levels were located mainly at the electron-donating TPA moieties, while the LUMO energy levels were generally located at the corresponding electron-withdrawing units. In the case of **6FPI** and **DSPI**, the distribution LUMO energy levels were within the dianhydride and imide ring moiety due to their strong electron-withdrawing capability. Compared to **6FPI** and **DSPI**, the distribution LUMO energy level of **6FPI′** was also located at the imide ring moiety. However, due to the direction of polyimide linkages between **6FPI′** and other polyimides is different, the HOMO and LUMO energy levels of **6FPI′** almost overlap and result in the poor sustaining ability for the CT complex. The LUMO energy levels of the polyesters and polyamides were found at the ester and amide linkage groups. However, the poorest charge separation phenomena of polyether **OXPE** and **DSPE** could be predicted and observed in the analysis of molecular simulation, indicating the weakest electron-withdrawing capability resulted from the isolated ether linkage group. Compared to other polymers, LUMO2 of **OXPE** and **DSPE** was distributed with overlapping around the whole basic unit that could also be indicated as evidence for the poor sustaining ability of the CT complex.

According to previous literature,[4a] when the applied electric fields reach the switching-on voltage, some electrons at the HOMO accumulate energy and transit to the LUMO5 (LUMO4

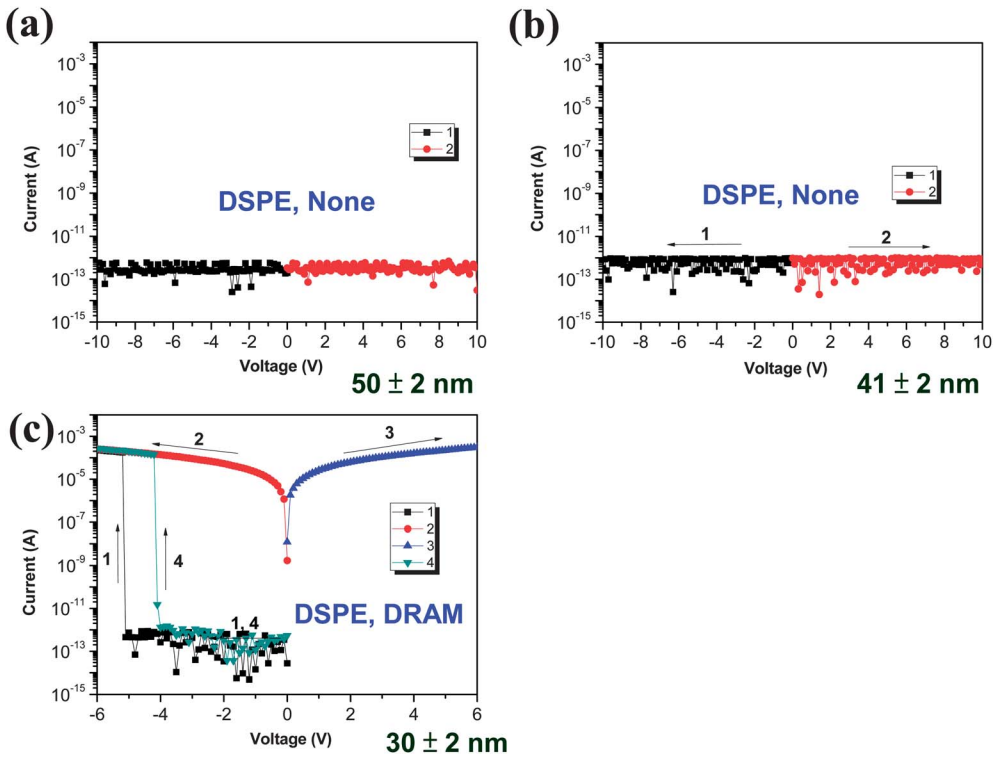

Fig. 6 Current–voltage (*I–V*) characteristics of the ITO/**DSPE**/Al memory device with different **OXPE** film thickness around (a) 50 nm, (b) 40 nm and (c) 30 nm.

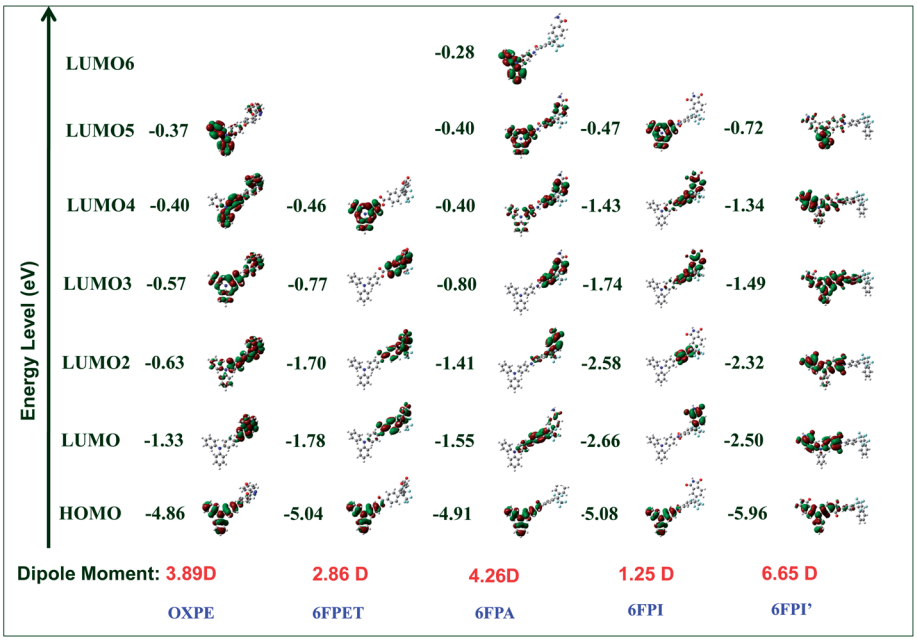

Fig. 7 Calculated molecular orbitals and the corresponding energy levels of the basic units (BU) for **OXPE**, **6FPET**, **6FPA**, **6FPI**, and **6FPI'**.

for **6FPET**) with the highest probability because of overlapping of the HOMO and LUMO5 resulting in an excited state. In addition, electrons at the HOMO can also be excited to other intermediate LUMOs with lower energy barrier belonging to the acceptor units. Thus, CT occurs through several courses to form the conductive CT complexes, including indirectly from the LUMO5 through intermediate LUMOs and then to the LUMO, or from the intermediate LUMOs to the LUMO, and directly from the HOMO to the LUMO. Based on this proposed mechanism, when the negative sweep was conducted, the hole injected from the bottom electrode ITO to the HOMO of the polymer due to the lower band gap between ITO (−4.8 eV) and HOMO.[16] In

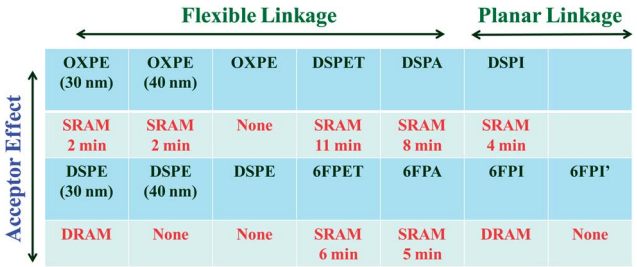

Fig. 8 Memory properties of TPA-based aromatic polymers. A standard thickness (50 nm) of polymer film was used without specific mention.

contrast, during the positive sweep, the hole is difficult to be injected from the top electrode Al into the HOMO of these polymers because of the larger energy gap between the work function of Al (−4.2 eV) and HOMO of the polymers, thus the memory device could not be switched to the ON state.

Furthermore, the stability of the CT complex is important and is related to the retention time of the memory device. Therefore, **OXPE** and **DSPE** showed only insulator behavior with 50 nm thickness due to the large band gap and weak CT capability. Compared to **DSPE**, **OXPE** with a stronger acceptor oxdiazole moiety revealed a longer retention time (SRAM) than **DSPE** (DRAM) in the case of decreasing thickness to 30 nm. In addition, **6FPA** exhibited a longer retention time than **6FPI** contributing to the conformation effect and higher dipole moment. The conformation of the phenyl ring with amide linkage is not a planar structure which may block the back CT occurring, and the higher dipole moment of **6FPA** also facilitates to stabilize the CT complex. **6FPET** having a similar non-planar structure to **6FPA** but lower LUMO than **6FPA** leads to even longer retention time than **6FPA**. As described before, the HOMO and LUMO charge density isosurfaces of **6FPI′** almost overlap and result in the poor sustaining ability for the CT complex. Therefore, although the chemical structure of **6FPI′** was similar to **6FPI**, **6FPI′** only has insulator behavior. The memory properties of TPA-based aromatic polymers are summarized in Fig. 8. Generally, polymers with flexible linkages, lower LUMO energy levels, and higher dipole moments will facilitate the stability of the CT complex, and the retention time of polymer memory devices is very dependent on the stability of the CT complex. Therefore, the sulfonyl-containing polymers generally show a longer retention time than 6F series polymers with the same linkages due to the stronger acceptor effect. For example, **DSPI** possesses SRAM property while **6FPI** has DRAM property. **DSPET** and **DSPA** have a longer retention time than **6FPET** and **6FPA**, respectively.

Conclusion

In summary, a new functional TPA-based aromatic polyether **OXPE** and polyester **6FPET** were successfully synthesized for the first time for memory device applications. For comparison, **6FPA**, **6FPI**, and **6FPI′** were also prepared for systematically investigating the relationship between the chemical structure and memory behavior. To get more insight into the acceptor effect on memory behavior, sulfonyl-containing polymers were also added into the discussion. **OXPE** exhibited the 2 minutes retention time SRAM property with thickness 30 and 40 nm, while **DSPE** exhibited only DRAM behavior when the film thickness was reduced to 30 nm. **6FPET** and **6FPA** showed SRAM properties with different retention times of 6 min, and 5 min, respectively. **6FPI** with a planar linkage group exhibited DRAM behavior while the corresponding isomer **6FPI′** showed insulator characteristic due to the difficulty in sustaining the charge transfer complex. Furthermore, sulfonyl-containing polymers generally have a longer retention time than 6F series polymers with the same linkage due to the stronger acceptor effect.

Experimental

Materials

4,4′-Dihydroxytriphenylamine (**1**),[14a] 4,4′-diaminotriphenylamine (**2**),[14b] *N*,*N*-bis(3,4-dicarboxyphenyl)aniline dianhydride (**3**),[14c] 2,5-bis(4-fluorophenyl)-1,3,4-oxadiazole (**OXDF**),[14d] and 4,4′-(hexafluoroisopropylidene)bis(benzoyl chloride) (**6FAC**)[14e] were synthesized according to previous literature. The electroactive TPA-based aromatic polyamide **6FPA**[15a] and polyimides **6FPI**[15b] and **6FPI′**[14c] were also prepared according to previous research. Acetonitrile (CH_3CN) (ACROS), *N*,*N*-dimethylacetamide (DMAc) (TEDIA), *N*-methyl-2-pyrrolidinone (NMP) (TEDIA), *o*-dichlorobenzene (TEDIA) and *m*-cresol (Alfa Aesar) were used without further purification. 2,2-Bis(3,4-dicarboxyphenyl)hexafluoropropane dianhydride (6FDA) (Chriskev) was purified by vacuum sublimation. Tetrabutylammonium perchlorate (TBAP) (ACROS) was recrystallized twice by ethyl acetate under nitrogen atmosphere and then dried *in vacuo* prior to use. All other reagents were used as received from commercial sources.

Preparation of polyether OXPE

A three necked 50 mL glass reactor was filled with diol monomer **1** (0.14 g, 0.5 mmol), **OXDF** (0.13 g, 0.5 mmol), 1.5 mL NMP, 1 mL toluene, and an excess of potassium carbonate (0.15 g, 0.75 mmol). The reaction mixture was heated at 150 °C for 3 h to remove water during the formation of phenoxide anions, and then heated at 170 °C for 1 h, 180 °C for 3 h, and finally heated at 190 °C for 1 h. After the reaction, the obtained polymer solution was poured slowly into 300 mL of acidified methanol–water (v/v = 1/1). The precipitate was collected by filtration, washed thoroughly with hot water and methanol, and dried under vacuum at 100 °C. The inherent viscosity and weight-average molecular weight (M_w) of the obtained polyether **OXPE** were 0.29 dL g^{-1} (measured at a concentration of 0.5 g dL^{-1} in DMAc at 30 °C) and 62 000, respectively. The FT-IR spectrum of the **OXPE** film exhibited characteristic C=N stretching absorption bands at around 1500–1600, and 1232 cm^{-1} (C–O–C stretching).

Preparation of polyester 6FPET

A mixture of 0.15 g (0.53 mmol) diol monomer **1** and 0.18 g (0.53 mmol) **6FAC** in 1.5 mL of *o*-dichlorobenzene was heated

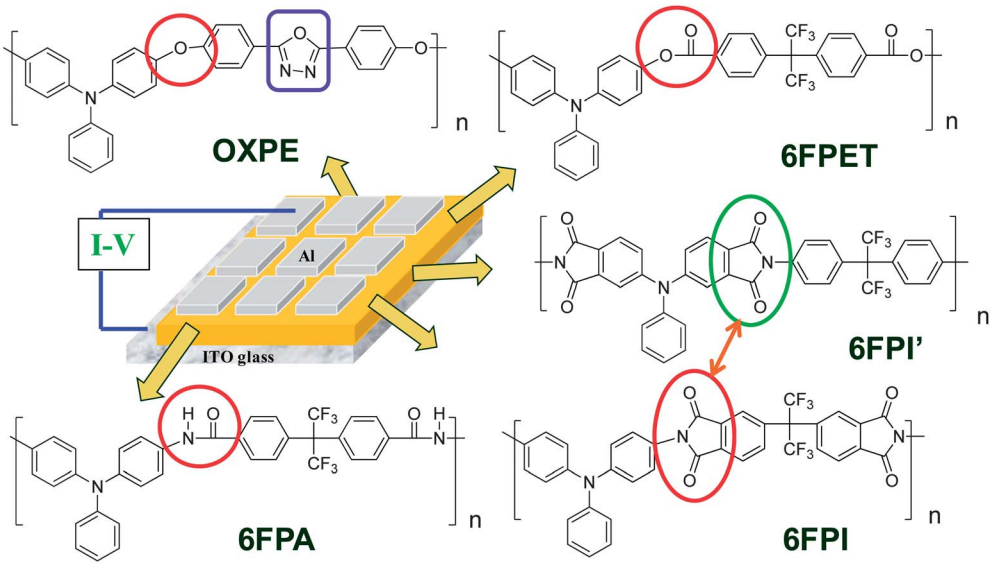

Scheme 1 Chemical structures of TPA-based aromatic polymers and the schematic diagram of the memory device consisting of a polymer thin film sandwiched between an ITO bottom electrode and an Al top electrode.

with stirring at 180 °C for 15 h under nitrogen. The solution thus obtained was poured into 300 mL of methanol. The yield of the polymer was 0.29 g (98%), and the inherent viscosity was 0.27 dL g^{-1} in DMAc. The weight-average molecular weight (M_w) of **6FPET** was 76 000. The IR spectrum (film) showed an absorption at 1737 cm^{-1} (C=O).

Polymer properties measurements

Fourier transform infrared (FT-IR) spectra were recorded on a PerkinElmer Spectrum 100 Model FT-IR spectrometer. The inherent viscosities were determined at 0.5 g dL^{-1} concentration using a Tamson TV-2000 viscometer at 30 °C. Gel permeation chromatographic (GPC) analysis was carried out on a Waters chromatography unit interfaced with a Waters 2410 refractive index detector. Two Waters 5 μm Styragel HR-2 and HR-4 columns (7.8 mm I. D. × 300 mm) were connected in series with NMP as the eluent at a flow rate of 0.5 mL min^{-1} at 40 °C and were calibrated with polystyrene standards. Thermogravimetric analysis (TGA) was conducted with TA SDT Q600. Experiments were carried out on approximately 6–8 mg film samples heated in flowing nitrogen or air (flow rate = 20 cm^3 min^{-1}) at a heating rate of 20 °C min^{-1}. Differential scanning calorimetry (DSC) analyses were performed on a PerkinElmer Pyris 1 DSC at a scan rate of 10 °C min^{-1} in flowing nitrogen (20 cm^3 min^{-1}). Electrochemistry was performed with a CH Instruments 611B electrochemical analyzer. Voltammograms were presented with the positive potential pointing to the left and with increasing anodic currents pointing downwards. Cyclic voltammetry (CV) was conducted with a three-electrode cell in which ITO (polymer films with area about 0.5 cm × 1.1 cm) was used as a working electrode. A platinum wire was used as an auxiliary electrode. All cell potentials were measured using a homemade Ag/AgCl, KCl (sat.) reference electrode. UV-visible absorption was recorded on a UV-visible spectrophotometer (Hitachi U-4100).

Fabrication and measurement of the memory device

The memory device was fabricated with the configuration of ITO/polymer/Al as shown in Scheme 1. The ITO glass used for the memory device was cleaned by ultrasonication with water, acetone, and isopropanol each for 15 min. DMAc solutions of TPA-based aromatic polymers (15–25 mg mL^{-1}) were first filtered through a PTFE membrane syringe filter of 0.45 μm pore size. Then, 250 μL of the filtered solution was spin-coated onto the ITO glass at a rotation rate of 1000 rpm for 60 s and kept at 100 °C for 10 min under nitrogen. The thicknesses of thin films prepared by DMAc solutions with different polymer concentrations were determined using an alpha-step profilometer. A 300 nm thick Al top electrode was thermally evaporated through the shadow mask (recorded device units of 0.5 × 0.5 mm^2 in size) at a pressure of 10^{-7} Torr with a uniform depositing rate of 3–6 Å s^{-1}. The electrical characterization of the memory device was performed using a Keithley 4200-SCS semiconductor parameter analyzer equipped with a Keithely 4205-PG2 arbitrary waveform pulse generator. ITO was used as a common electrode and Al was the electrode for applying voltage during the sweep.

Molecular simulation

Molecular simulations in this study were carried out with the Gaussian 09 program package. Equilibrium ground state geometry and electronic properties of basic unit of TPA-based aromatic polymers were optimized by means of the density functional theory (DFT) method at the B3LYP level of theory (Beckes-style three-parameter density functional theory using the Lee–Yang–Parr correlation functional) with the 6-31G(d) basis set.

Acknowledgements

We gratefully acknowledge the financial support for this research through the National Science Council of Taiwan.

References and notes

1 (*a*) P. O. Sliva, G. Dir and C. Griffiths, *J. Non-Cryst. Solids*, 1970, **2**, 316–333; (*b*) Q. D. Ling, D. J. Liaw, C. X. Zhu, D. S. H. Chan, E. T. Kang and K. G. Neoh, *Prog. Polym. Sci.*, 2008, **33**, 917–978; (*c*) S. Moller, C. Perlov, W. Jackson, C. Taussig and S. R. Forrest, *Nature*, 2003, **426**, 166–169; (*d*) J. C. Scott and L. D. Bozano, *Adv. Mater.*, 2007, **19**, 1452–1463.

2 (*a*) A. Stikeman, *Technol. Rev.*, 2002, 31; (*b*) P. Heremans, G. H. Gelinck, R. Muller, K. J. Baeg, D. Y. Kim and Y. Y. Noh, *Chem. Mater.*, 2011, **23**, 341–358.

3 (*a*) B. Cho, T. W. Kim, S. Song, Y. Ji, M. Jo, H. Hwang, G. Y. Jung and T. Lee, *Adv. Mater.*, 2010, **22**, 1228–1232; (*b*) T. W. Kim, D. F. Zeigler, O. Acton, H. L. Yip, H. Ma and A. K. Y. Jen, *Adv. Mater.*, 2012, **24**, 828–833; (*c*) R. J. Tseng, J. X. Huang, J. Ouyang, R. B. Kaner and Y. Yang, *Nano Lett.*, 2005, **5**, 1077–1080; (*d*) C. X. Wu, F. S. Li, T. L. Guo and T. W. Kim, *Org. Electron.*, 2012, **13**, 178–183.

4 (*a*) Q. D. Ling, F. C. Chang, Y. Song, C. X. Zhu, D. J. Liaw, D. S. H. Chan, E. T. Kang and K. G. Neoh, *J. Am. Chem. Soc.*, 2006, **128**, 8732–8733; (*b*) C. L. Liou and W. C. Chen, *Polym. Chem.*, 2011, **2**, 2169–2174.

5 (*a*) X. D. Zhuang, Y. Chen, G. Liu, P. P. Li, C. X. Zhu, E. T. Kang, K. G. Noeh, B. Zhang, J. H. Zhu and Y. X. Li, *Adv. Mater.*, 2010, **22**, 1731–1735; (*b*) X. D. Zhuang, Y. Chen, B. X. Li, D. G. Ma, B. Zhang and Y. Li, *Chem. Mater.*, 2010, **22**, 4455–4461; (*c*) Y. G. Ko, W. Kwon, D. M. Kim, K. Kim, Y. S. Gal and M. Ree, *Polym. Chem.*, 2012, **3**, 2028–2033; (*d*) W. Lin, H. Sun, S. Liu, H. Yang, S. Ye, W. Xu, Q. Zhao, X. Liu and W. Huang, *Macromol. Chem. Phys.*, 2012, **213**, 2472–2478; (*e*) S. J. Liu, W. P. Lin, M. D. Yi, W. J. Xu, C. Tang, Q. Zhao, S. H. Ye, X. M. Liu and W. Huang, *J. Mater. Chem.*, 2012, **22**, 22964–22970; (*f*) S. Baek, D. Lee, J. Kim, S. H. Hong, O. Kim and M. Ree, *Adv. Funct. Mater.*, 2007, **17**, 2637–2644; (*g*) H. C. Wu, A. D. Yu, W. Y. Lee, C. L. Liu and W. C. Chen, *Chem. Commun.*, 2012, **48**, 9135–9137.

6 (*a*) B. Zhang, G. Liu, Y. Chen, C. Wang, K. G. Neoh, T. Bai and E. T. Kang, *ChemPlusChem*, 2012, **77**, 74–81; (*b*) S. J. Liu, P. Wang, Q. Zhao, H. Y. Yang, J. Wong, H. B. Sun, X. C. Dong, W. P. Lin and W. Huang, *Adv. Mater.*, 2012, **24**, 2901–2905; (*c*) S. G. Hahm, N. G. Kang, W. Kwon, K. Kim, Y. K. Ko, S. Ahn, B. G. Kang, T. Chang, J. S. Lee and M. Ree, *Adv. Mater.*, 2012, **24**, 1062–1066; (*d*) Y. K. Fang, C. L. Liu, G. Y. Yang, P. C. Chen and W. C. Chen, *Macromolecules*, 2011, **44**, 2604–2612; (*e*) S. J. Liu, P. Wang, Q. Zhao, H. Y. Yang, J. Wong, H. B. Sun, X. C. Dong, W. P. Lin and W. Huang, *Adv. Mater.*, 2012, **24**, 2901–2905.

7 (*a*) A. D. Yu, C. L. Liu and W. C. Chen, *Chem. Commun.*, 2012, **48**, 383–385; (*b*) D. B. Velusamy, S. K. Hwang, R. H. Kim, G. Song, S. H. Cho, I. Bae and C. Park, *J. Mater. Chem.*, 2012, **22**, 25183–25189; (*c*) B. Zhang, Y. Chen, G. Liu, L. Q. Xu, J. Chen, C. X. Zhu, K. G. Neoh and E. T. Kang, *J. Polym. Sci., Part A: Polym. Chem.*, 2012, **50**, 378–387; (*d*) M. A. Khan, U. S. Bhansali, D. Cha and H. N. Alshareef, *Adv. Funct. Mater.*, 2013, **23**, 2145; (*e*) J. C. Chen, C. L. Liu, Y. S. Sun, S. H. Tungd and W. C. Chen, *Soft Matter*, 2012, **8**, 526–535; (*f*) S. Gao, C. Song, C. Chen, F. Zeng and F. Pan, *J. Phys. Chem. C*, 2012, **116**, 17955–17959; (*g*) C. J. Chen, Y. C. Hu and G. S. Liou, *Chem. Commun.*, 2013, **49**, 2804–2806; (*h*) L. Q. Xu, B. Zhang, K. G. Neoh, E. T. Kang and G. D. Fu, *Macromol. Rapid Commun.*, 2013, **34**, 234–238; (*i*) M. A. Mamo, A. O. Sustaita, N. J. Coville and I. A. Hummelgen, *Org. Electron.*, 2013, **14**, 175–181.

8 (*a*) T. Kurosawa, Y. C. Lai, T. Higashihara, M. Ueda, C. L. Liu and W. C. Chen, *Macromolecules*, 2012, **45**, 4556–4563; (*b*) Y. Q. Li, R. C. Fang, A. M. Zheng, Y. Y. Chu, X. Tao, H. H. Xu, S. J. Ding and Y. Z. Shen, *J. Mater. Chem.*, 2011, **21**, 15643–15654; (*c*) T. J. Lee, Y. G. Ko, H. J. Yen, K. Kim, D. M. Kim, W. Kwon, S. G. Hahm, G. S. Liou and M. Ree, *Polym. Chem.*, 2012, **3**, 1276–1283; (*d*) F. Chen, G. Tian, L. Shi, S. Qi and D. Wu, *RSC Adv.*, 2012, **2**, 12879–12885; (*e*) Y. Liu, Y. Zhang, Q. Lan, S. Liu, Z. Qin, L. Chen, C. Zhao, Z. Chi, J. Xu and J. Economy, *Chem. Mater.*, 2012, **24**, 1212–1222; (*f*) T. Kurosawa, T. Higashihara and M. Ueda, *Polym. Chem.*, 2013, **4**, 16–30; (*g*) N. H. You, C. C. Chueh, C. L. Liu, M. Ueda and W. C. Chen, *Macromolecules*, 2009, **42**, 4456–4463; (*h*) S. G. Hahm, S. Choi, S. H. Hong, T. J. Lee, S. Park, D. M. Kim, W. S. Kwon, K. Kim, O. Kim and M. Ree, *Adv. Funct. Mater.*, 2008, **18**, 3276–3282; (*i*) Q. Liu, K. Jiang, Y. Wen, J. Wang, J. Luo and Y. Song, *Appl. Phys. Lett.*, 2010, **97**, 253304; (*j*) Y. Li, Y. Chu, R. Fang, S. Ding, Y. Wang, Y. Shen and A. Zheng, *Polymer*, 2012, **53**, 229–240.

9 (*a*) C. J. Chen, H. J. Yen, W. C. Chen and G. S. Liou, *J. Mater. Chem.*, 2012, **22**, 14085–14093; (*b*) T. J. Lee, C. W. Chang, S. G. Hahm, K. Kim, S. Park, D. M. Kim, J. Kim, W. S. Kwon, G. S. Liou and M. Ree, *Nanotechnology*, 2009, **20**, 135204; (*c*) D. M. Kim, S. Park, T. J. Lee, S. G. Hahm, K. Kim, J. C. Kim, W. Kwon and M. Ree, *Langmuir*, 2009, **25**, 11713–11719; (*d*) Y. C. Hu, C. J. Chen, H. J. Yen, K. Y. Lin, J. M. Yeh, W. C. Chen and G. S. Liou, *J. Mater. Chem.*, 2012, **22**, 20394–20402; (*e*) K. Kim, H. J. Yen, Y. G. Ko, C. W. Chang, W. Kwon, G. S. Liou and M. Ree, *Polymer*, 2012, **53**, 4135–4144; (*f*) Y. G. Ko, W. Kwon, H. J. Yen, C. W. Chang, D. M. Kim, K. Kim, S. G. Hahm, T. J. Lee, G. S. Liou and M. Ree, *Macromolecules*, 2012, **45**, 3749–3758; (*g*) T. J. Lee, Y. G. Ko, H. J. Yen, K. Kim, D. M. Kim, W. Kwon, S. G. Hahm, G. S. Liou and M. Ree, *Polym. Chem.*, 2012, **3**, 1276–1283; (*h*) K. Kim, S. Park, S. G. Hahm, T. J. Lee, D. M. Kim, J. C. Kim, W. Kwon, Y. G. Ko and M. Ree, *J. Phys. Chem. B*, 2009, **113**, 9143–9150; (*i*) K. L. Wang, Y. L. Liu, J. W. Lee, K. G. Neoh and E. T. Kang, *Macromolecules*, 2010, **43**, 7159–7164; (*j*) Y. Li, R. Fang, S. Ding and Y. Shen, *Macromol. Chem. Phys.*, 2011, **212**, 2360–2370; (*k*) K. L. Wang, Y. L. Liu, I. H. Shih, K. G. Neoh and E. T. Kang, *J. Polym. Sci., Part A: Polym. Chem.*, 2010, **48**, 5790–5800; (*l*) A. D. Yu, T. Kurosawa, Y. C. Lai, T. Higashihara, M. Ueda, C. L. Liu and W. C. Chen, *J. Mater. Chem.*, 2012, **22**, 20754–20763; (*m*) D. M. Kim, Y. G. Ko, J. K. Choi, K. Kim, W. Kwon, J. Jung, T. H. Yoon and M. Ree, *Polymer*, 2012, **53**, 1703–1710.

10 (*a*) C. W. Chang, G. S. Liou and S. H. Hsiao, *J. Mater. Chem.*, 2007, **17**, 1007–1015; (*b*) H. J. Yen and G. S. Liou, *Chem. Mater.*, 2009, **21**, 4062–4070; (*c*) H. J. Yen, H. Y. Lin and G. S. Liou, *Chem. Mater.*, 2011, **23**, 1874–1882; (*d*) G. S. Liou, C. W. Chang, H. M. Huang and S. H. Hsiao, *J. Polym. Sci., Part A: Polym. Chem.*, 2007, **45**, 2004–2014.

11 (*a*) C. J. Chen, H. J. Yen, W. C. Chen and G. S. Liou, *J. Polym. Sci., Part A: Polym. Chem.*, 2011, **49**, 3709–3718; (*b*) C. J. Chen, Y. C. Hu and G. S. Liou, *Chem. Commun.*, 2013, **49**, 2536–2538.

12 (*a*) Y. L. Liu, K. L. Wang, G. S. Huang, C. X. Zhu, E. S. Tok, K. G. Neoh and E. T. Kang, *Chem. Mater.*, 2009, **21**, 3391–3399; (*b*) T. Kuorosawa, C. C. Chueh, C. L. Liu, T. Higashihara, M. Ueda and W. C. Chen, *Macromolecules*, 2010, **43**, 1236–1244; (*c*) B. L. Hu, F. Zhuge, X. J. Zhu, S. S. Peng, X. X. Chen, L. Pan, Q. Yan and R. W. Li, *J. Mater. Chem.*, 2012, **22**, 520–526.

13 (*a*) G. S. Liou, H. J. Yen and M. C. Chiang, *J. Polym. Sci., Part A: Polym. Chem.*, 2009, **47**, 5378–5385; (*b*) H. J. Yen and G. S. Liou, *Org. Electron.*, 2010, **11**, 299–310.

14 (*a*) M. Faccini, M. Balakrishnan, M. B. J. Diemeer, R. Torosantucci, A. Driessen, D. W. Reinhoudt and W. Verboom, *J. Mater. Chem.*, 2008, **18**, 5293–5300; (*b*) Y. Oishi, H. Takado, M. Kakimoto and Y. Imai, *J. Polym. Sci., Polym. Chem. Ed.*, 1990, **28**, 1763–1769; (*c*) W. Li, S. Li, Q. Zhang and S. Zhang, *Macromolecules*, 2007, **40**, 8205–8211; (*d*) J. L. Hedrick and R. Twieg, *Macromolecules*, 1992, **25**, 2021–2025; (*e*) C. S. Wu, S. L. Lee and Y. Chen, *J. Polym. Sci., Part A: Polym. Chem.*, 2011, **49**, 3099–3108.

15 (*a*) S. H. Cheng, S. H. Hsiao, T. H. Su and G. S. Liou, *Macromolecules*, 2005, **38**, 307–316; (*b*) H. Su, S. H. Hsiao and G. S. Liou, *J. Polym. Sci., Part A: Polym. Chem.*, 2005, **43**, 2085–2098.

16 Q. D. Ling, Y. Song, S. L. Lim, E. Y. H. Teo, Y. P. Tan and C. X. Zhu, *Angew. Chem., Int. Ed.*, 2006, **45**, 2947–2951.